

Performance analysis of voltage source converter based high voltage direct current line under small control perturbations

Reem Ahmed Mostafa¹, Adel Emary Salem², Ahmed Sayed Abdelhamid¹,
Mohamed EL-Shimy Mahmoud Bekhet³

¹Department of Electrical Power and Machines Engineering, The Higher Institute of Engineering, El'Shorouk City, Egypt

²National Energy Control Center–Egyptian Electricity Transmission Company, Cairo, Egypt

³Department of Electrical Power and Machines Engineering, Ain Shams University (ASU), Cairo, Egypt

Article Info

Article history:

Received Feb 27, 2023

Revised Aug 20, 2023

Accepted Sep 3, 2023

Keywords:

Control strategies

HVDC transmission system

Insulated-gate bipolar transistor

MATLAB Simulink

Voltage source converter

VSC-HVDC

ABSTRACT

High voltage direct current (HVDC) systems provide important advantages; among them the ability to transmit enormous amounts of electrical power over great distances at low cost. As a result, planners of power systems consider it as a viable choice for power transmission and interconnection of asynchronous networks. Depending on HVDC grids, continental/super grids have been recently constructed to promote global economic development. The study described in the paper focuses on the behavior of a voltage sourced converter (VSC) based HVDC transmission system comprising three arms-neutral point clamped (NPC) converters interconnecting two asynchronous alternating current (AC) networks. In addition, the system components, and the vector control strategy of active/reactive powers and direct current (DC) bus voltage are simulated in MATLAB/Simulink under varying situations by adjusting the controller's settings. The study records and analyzes AC/DC voltages and active/reactive powers at two converter stations under varying power and voltage conditions. The results of the study provide key performance indicators, such as settling time (tsett), steady state error (SSE), overshoot/undershoot (OS%/US%), and correlation factor (CF), which demonstrate the robustness of the system's control.

This is an open access article under the [CC BY-SA](https://creativecommons.org/licenses/by-sa/4.0/) license.



Corresponding Author:

Reem Ahmed Mostafa

Department of Electrical Power and Machines Engineering, The Higher Institute of Engineering

El'Shorouk City, Egypt

Email: reem.ahmed.mos@gmail.com

1. INTRODUCTION

Recently, there is an increasing need for both broad usage of renewable energy sources and active power distribution networks all over the world. Additionally, there has been an increase in global support for interconnecting electrical systems. High voltage direct current (HVDC) transmission systems are a viable alternative since they permit the integration of renewable energy sources with passive networks and facilitate asynchronous grid connectivity. Consequently, the demand for HVDC transmission systems is growing, necessitating multi-terminal HVDC transmission systems whose forming which known as super grids [1]–[3].

Currently, “super grid” term refers to the connection of both local power generation and remote renewable energy sources with the populated sites through a continental or transcontinental network. Many super grids have grown because of the increased environmental issues and the recent developed technologies. These schemes integrate several technologies such as monitoring, control, and communication. For example, the Asian super grid interconnects many countries in Northeast Asia like Korea, China, Japan, Russia, and others. To connect these countries of different frequencies, HVDC transmission systems are used due to their

capability to transmit bulk power over long distances between asynchronous networks, unlike HVAC transmission which cannot directly connect asynchronous systems [4], [5].

The primary responsibility of multi-terminal HVDC transmission systems is to establish control strategies for power distribution that match the requirements of each terminal. In recent years, a growing number of studies have been conducted to investigate the control strategies of such systems, including DC voltage droop control and master-slave control [6], [7]. However, more investigations are needed due to the complexity and diversity of the existing control strategies that arise from the various requirements of AC systems at each terminal.

HVDC transmission systems commonly use two basic technologies: HVDC based on “line-commutated converters” (LCC-HVDC) and HVDC based on “voltage-sourced converters” (VSC-HVDC). A significant number of reactive power adjustment devices are needed with LCC-HVDC converter. When the flow of the power is reversed, the polarity of the LCC voltage must be altered. Therefore, it is challenging to create a multi-terminal HVDC transmission for LCC. VSC-HVDC equipment has a smaller footprint area and a more compact construction than LCC-HVDC equipment since it does not need reactive power compensation. In addition, the LCC-HVDC system is susceptible to commutation failure, but the VSC-HVDC system does not face this danger due to the insulated-gate bipolar transistor (IGBT) technology. Nevertheless, the existing VSC-HVDC transmission system has limitations such as high prices, significant operating losses, and limited capacity. In addition, multiple restrictions on the VSC-based HVDC have been discovered; these restrictions are most apparent when the direct current (DC) system is linked to a very weak alternating current (AC) grid due to the difficulty in providing reactive power at the appropriate rate when a fault happens [8], [9]. This results in high voltage distortion and improper operation of that converter, resulting in sluggish system recovery. As a result, numerous VSC-HVDC transmission system control strategies have been investigated as potential solutions to the issues. In addition, the HVDC design is intended to further improve the system’s adaptability to unforeseen conditions, making it easier to maintain control and stability. In order to obtain the output frequency of the inverter, and ensure exact and accurate active and reactive powers, VSC-HVDC must be under strict control.

In this study, we analyze how the VSC-HVDC system reacts to changes in DC voltage, active power, and reactive power. These manipulated variables are subjected to disturbances in the form of step inputs. The transient response of each station converter is then analyzed by continuously monitoring the active/reactive power waveforms and the AC/DC voltage waveforms.

2. VSC-HVDC TRANSMISSION SYSTEM LAYOUT

Figure 1 shows a typical configuration of the HVDC transmission system based VSC. The AC source (1) is an AC network transmitting side while AC source (2) is an AC network receiving end. The voltage and frequency of the AC networks, sources (1) and (2), may vary. The AC waveform from AC source (1) is rectified into a DC waveform by control station 1 (VSC1), which is a converter. A DC transmission line will then transmit the DC voltage to a second converter, an inverter, at control station 2 (VSC2), which will manage the DC link voltage and reverse the DC waveform to AC.

IGBT is the VSC’s primary operational component. It is the most widely used transistor as it combines the favourable properties of the bipolar transistors and metal oxide semiconductor field effect transistors (MOSFETs) as well. In a VSC, the IGBT switching valves have higher input impedance, smaller on-state voltage drops, and longer turn-off time than MOSFETs. In addition, IGBT is highly controllable, has a greater switching frequency, and may generate an output voltage with any desired amplitude or phase angle [10].

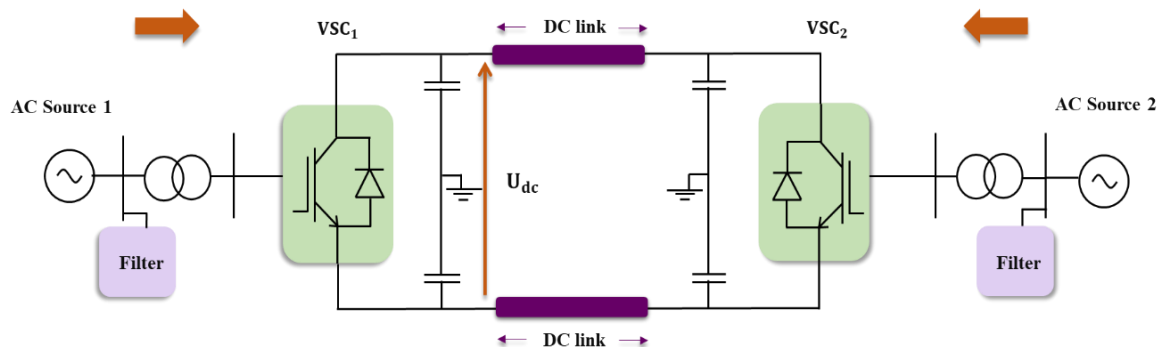


Figure 1. VSC-HVDC system interconnecting two AC sources

3. VARIOUS CATEGORIES OF HVDC SYSTEMS BASED ON VSC

Several VSC layouts have been upgraded to be utilized in a wide range of industries. Generally, VSCs may be classified based on their configurations into several classes including two-level, three-level, and modular multilevel converters (MMC) [11]. However, the existing converters face many challenges that need to be overcome. Consequently, new technologies will be invented to produce an enhanced and more efficient VSC model.

3.1. Configuration 1: two-level converter

In three-phase systems, a two-level converter is also called a six-pulse bridge. The main components of this converter are IGBTs equipped with reverse parallel diodes, and DC capacitors. As illustrated in Figure 2, the output AC voltage for each phase operates within two distinct voltage levels relative to the positive and negative terminals of DC voltage. To decrease the converter's harmonic distortion, this kind of VSC converter relies on pulse width modulation (PWM) method which leads to large switching losses. These losses are caused by the repeated (usually twenty) on-and-off switching of the IGBT, which reduces the transmission's overall efficiency. In addition, the simultaneous switching of IGBTs linked in series would necessitate an extremely high operating voltage, which might lead to electromagnetic interference issues [10].

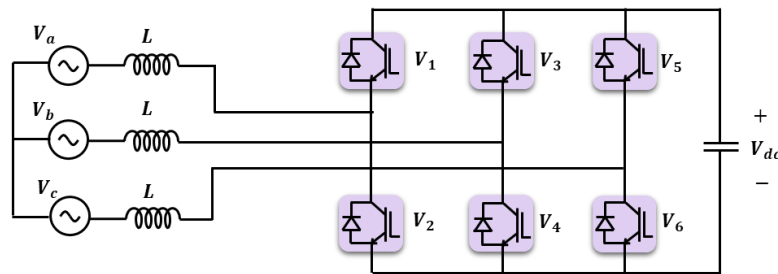


Figure 2. Two-level VSC connected to HVDC link

3.2. Configuration 2: three-level converter

The three-level converter contributes substantially to the enhancement of the harmonic performance of the converter. This is done by employing three distinct voltage levels for each phase of the AC waveform according to Figure 3. The DC capacitor is separated into two sections where the diode valves are linked between the midpoint of the capacitors for one phase and the quarter and three-quarter points for the other two phases [12], [13].

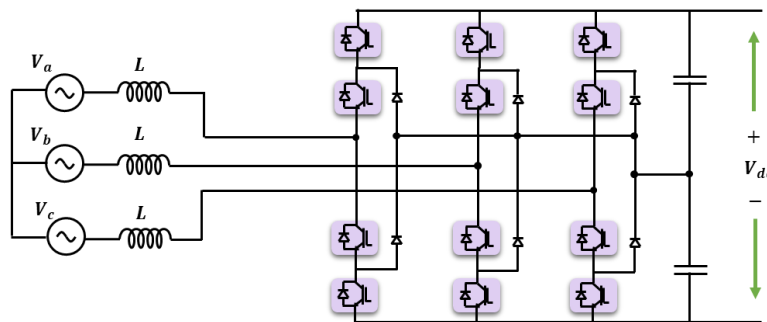


Figure 3. Three-level neutral-point diode-clamped (NPC) VSC connected to HVDC link

3.3. Configuration 3: modular multilevel converter

MMC consists of six valves fitted inside three sub-modules (SMs) as same as the two-level converter. Each valve links two legs: DC and AC similar to a two-level converter [14]–[17]. In MMC, however, each valve is equipped with its own voltage source, and a capacitor used for storage. Each SM consists of two IGBTs connected in series across the capacitor, with their common terminal linked to the AC source [16]. The structure of modular multilevel VSC involving its submodule representation is demonstrated in Figure 4.

The two IGBTs included in each SM are independently turned on. During the switching on mode, the IGBT links the capacitor to the circuit. In contrast to the on- state condition, the IGBT bypasses the capacitor during the switching off mode. Therefore, the voltage produced by each sub-module may be either zero or sub-module capacitor voltage, V_c . Thus, by connecting an adequate number of series sub-modules, the valve may produce voltage waveforms that are extremely near to a sine wave [14], [18]. Harmonic distortion in such a waveform will be very low [18]. VSC-HVDC systems utilizing MMC provide an outstanding harmonic performance without the requirement for either a filter or a PWM approach, which is one of MMC benefits [19]. In addition, the power losses are far less than the two-level converter. Despite these advantages, MMC has a few flaws such as a more complicated control than a two-level converter. In addition, due to the size of each sub-module in the capacitor, MMC size is bigger than that of a two-level converter, necessitating additional substation area [14], [19].

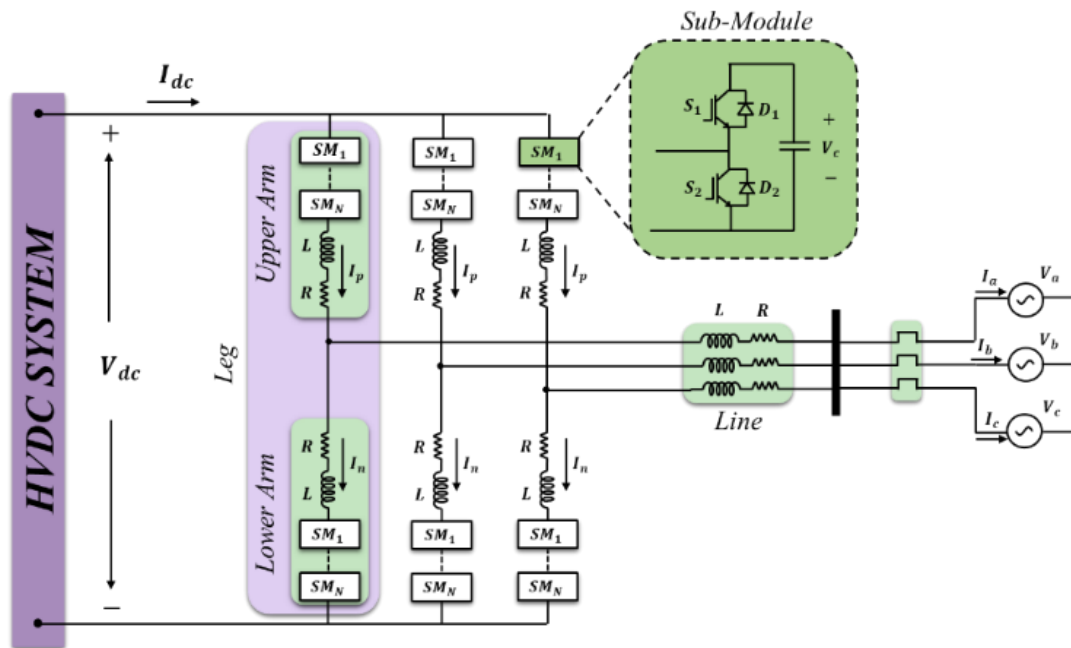


Figure 4. MMC-VSC connected to HVDC link

4. CONFIGURATION AND MATHEMATICAL MODELING

In Figure 5, a typical schematic diagram of the detailed MATLAB model of a modified VSC-HVDC transmission system used in this paper is shown, depicting the interconnection of two 230 kV, 2000 MVA AC systems with differing frequencies through an HVDC transmission system. The first source has a frequency of 50 Hz, whereas the second has a frequency of 60 Hz. Both AC systems, represented by damped L-R equivalents, are interfaced with the HVDC system through two identical VSC stations [20]. Each converter station employs a three-level NPC converter, as seen in Figure 3, as they are widely applied in industrial fields since they minimize the losses to 1.7% and cause negligible harmonics [21], [22]. NPC converter is comprised of insulated gate bipolar transistors and diodes due to their unique features. One converter station acts as a rectifier and the other as an inverter, depending on the power flow and voltage profile of each station. In order to transfer DC power, they are linked through 75 km HVDC cables, each one comprises of two pi sections according to Figure 5 [20]. As the reference power fluctuates frequently, oscillations should be reduced during electrical power transfer between the two systems. In addition, keeping DC voltage within allowable limits should be considered. Consequently, the VSC of each converter station must be controlled [23].

Figure 6 depicts the VSC-HVDC control scheme, which allows the DC voltage, active power, and reactive power of each converter station to be controlled. Since each AC supply is connected to the AC side of NPC converter station, the drawn active and reactive powers of the converter can be calculated according to (1) and (2) where the harmonics and reactance losses are neglected [24].

$$P_{VSC} = \frac{V_s \sin(\delta)}{X} V_c \tag{1}$$

$$Q_{VSC} = \frac{[V_s \cos(\delta) - V_c]}{X} V_c \tag{2}$$

Where V_s is the AC source voltage, V_c is the AC voltage measured at the AC side of the converter, X is the inductive reactance of the reactor, and δ is the phase shift between the two voltages V_s and V_c .

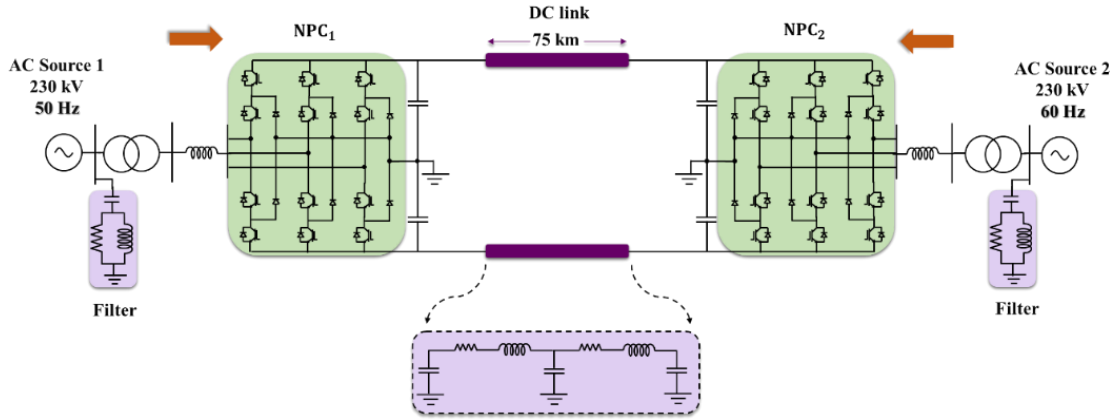


Figure 5. Schematic diagram of the detailed MATLAB model of a modified VSC-HVDC transmission

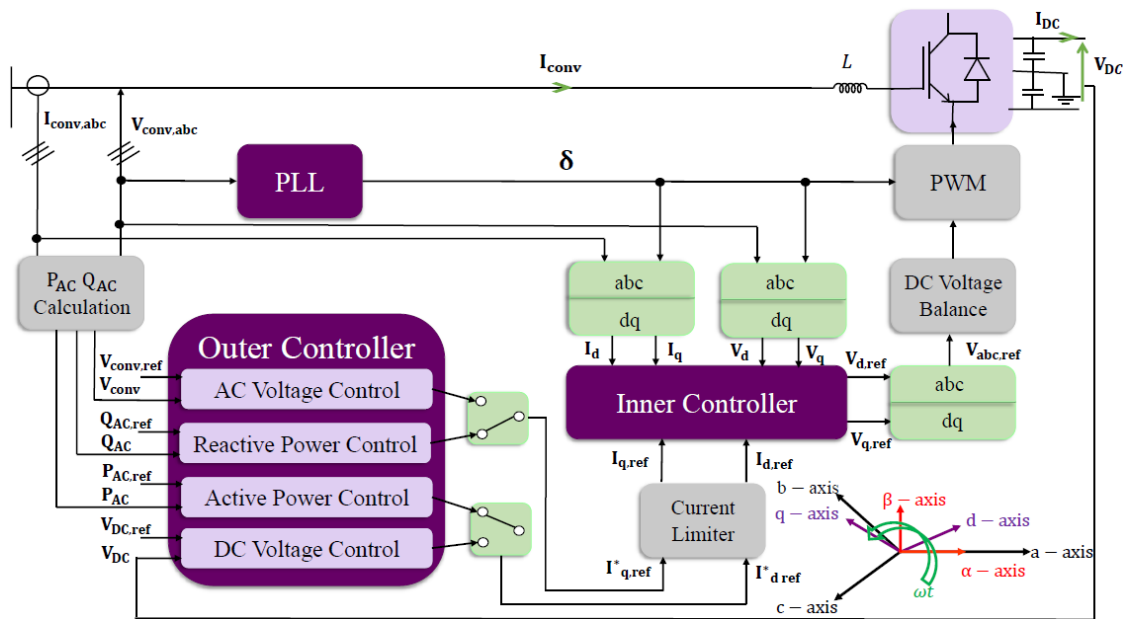


Figure 6. Vector current control (VCC) of modular multilevel VSC converter

Although there are a number of control technologies that may be used in VSC applications, the most prevalent is DQ control, which relies on translating the perceived stationary three-phase AC voltages and currents into a rotating dq domain [25], [26]. The outer loop of the controller is responsible for selecting the necessary control mode. The quadrature component of the current determines whether reactive power control or AC voltage control is required, whereas the direct component determines if DC voltage control or active power control is desired. This loop's output is the reference direct and quadrature components of the current $I_{d,ref}$, $I_{q,ref}$, respectively, which are the inputs of the inner control loop, which generates the reference voltage waveforms required for pulse width modulation (PWM) of the converter V_{ref} . phase locked loop (PLL) also gives the reference angle of the park's transformation that will be utilized in the inner current loop and aligns the d-axis with the voltage at the point of common coupling (PCC) [26]. The DC voltage balance control is

provided to maintain the DC side of the converter balanced in steady state since small deviations between the pole voltages can be resulted from active/reactive converter current variations, or errors of PWM control [20]. As depicted in Figure 7, the midpoint DC current (I_{d0}) assigns the U_{d0} value between the upper and lower DC poles. I_{d0} can be modulated by adjusting the conduction time of the switches in a pole, hence the voltage difference U_{d0} is controlled. For example, reducing a positive U_{d0} voltage difference to zero can be performed by increasing the set point voltage value which generates a positive I_{d0} . On the other hand, a negative I_{d0} requires decreasing the reference voltage value. This process can be achieved by adding an offset component to the sinusoidal reference voltage waveform. Thus, the activation of DC voltage balance function, at the converter station where the DC voltage is adjusted, provides proper performance [20]. According to (3) illustrates the relation between I_{d0} , U_{d1} , and U_{d2} .

$$I_{d0} = -C \frac{d}{dt} U_{d1} = -C \frac{d}{dt} (U_{d1} - U_{d2}) = -(I_{d1} + I_{d2}) \tag{3}$$

Where I_{d0} is the DC current at the midpoint, U_{d1} is the DC voltage across the first capacitive element, while U_{d2} is the DC voltage across the other capacitive element, and C is the capacitance of the DC link connected to the converter station see Figure 7.

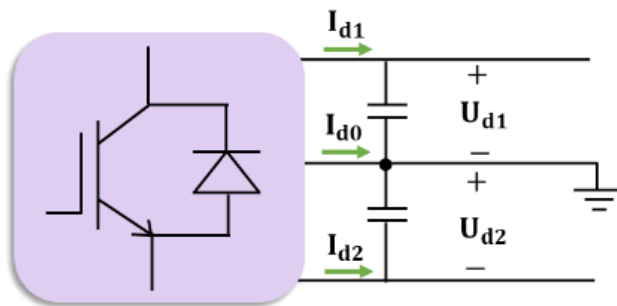


Figure 7. DC voltages and currents of a VSC based three-level NPC

5. CASE STUDY AND SIMULATION RESULTS

To examine the performance of the VSC-HVDC system under various disturbances, a modified MATLAB model including two 3-level converter stations with one set to active-reactive powers (P-Q) control mode and the other to reactive power-DC voltage (Q-U_{dc}) control mode will be used. Consequently, disturbances may be applied to the following variables: the reference active power of the first station $P_{ref.1}$, the reactive power at the first converter station $Q_{ref.1}$, and the reference dc voltage is applied at the second converter station $U_{d-ref.2}$. In order to determine the model's starting time, it is first run initially without any disturbances; then, a disturbance consisting of a-0.1 pu step input is applied individually to each of $P_{ref.1}$, $Q_{ref.1}$ and $U_{d-ref.2}$ at $t=1.5$ seconds. At both converter stations, waveforms of active/reactive powers and DC/AC voltages are recorded. In all case studies, transient response analysis is undertaken by determining the following parameters: percentage of maximum overshoot/undershoot (MPOS%/US%) and their occurring time (t_{max}/t_{min}) in seconds. In addition, the settling time (t_{sett}), or the time required to attain the steady state condition measured from the instant the disturbance occurred, is also measured in seconds since it is primarily influenced by the overshoot/undershoot. In each scenario, the steady state error (SSE) per unit is also determined. The correlation factor (CF) is used in this study to figure out how far apart the measured waveforms and the predicted actual (reference) waveforms are.

5.1. Model preparation

As mentioned before, the main purpose of this step is to estimate the onset time of the disturbances that will be applied to the studied model. Thus, the model will run without disturbances (model initialization) and capture the required waveforms. Figure 8 illustrates the initial response of the model before applying any perturbation to deduce the time taken by the system to reach the steady state. The behavior of the active power at each converter station is shown in Figure 8(a) while the reactive power response is illustrated in Figure 8(b). Additionally, the waveforms of the RMS AC voltage and DC voltage at each converter station are shown in Figures 8(c) and 8(d) respectively. As depicted in Figure 8, each recorded waveform at both converter stations takes about 1.2 sec. until it reaches the steady state value. As a result, the starting time of the model disturbances

will be taken as 1.2 sec. The interval from zero to 1.2 sec. will be excluded from the following upcoming results, as they are associated with the model initialization.

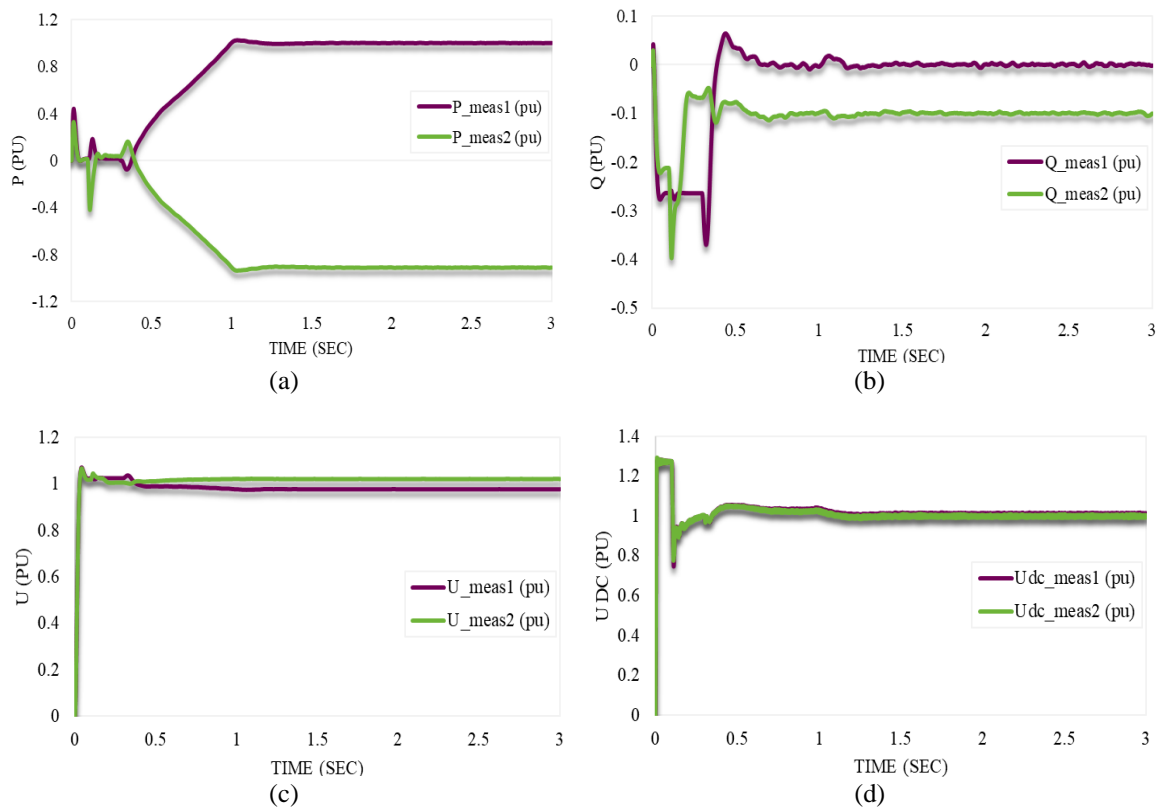


Figure 8. The measured: (a) active power, (b) reactive power, (c) RMS AC voltage, and (d) DC voltage at each converter station for the initial response of the VSC-HVDC transmission system

5.2. Case 1: applied disturbance in the reference active power of station 1 (Pref.1)

In this case, a disturbance on the active power of station 1 is applied, and the response at each converter station is analyzed. Figure 9 illustrates the response of active power, reactive power, RMS AC voltage and DC voltage at each converter station. Table 1 lists the transient response analysis of Pref.1 disturbance. As shown in Figure 9(a), with a 17% undershoot after the applied disturbance, P_{meas.1} rapidly reverts to its steady state with a far less steady state error than the other station see Table 1. Furthermore, the correlation factor of 0.9699 between Pref.1 and P_{meas.1} implies that the two waveforms behave in the same way. P_{meas.2}'s reaction to the same disturbance is counteracted by an overshoot of 12.5% and a lengthier time to achieve steady state, compared to P_{meas.1}. On the other hand, Q_{meas.1} responds with an overshoot of 3.8%, while Q_{meas.2} decreases to an undershoot of 16%, in contrast to the responses of the active powers see Table 1. In addition, Q_{meas.2} requires an extra 0.5 seconds beyond Q_{meas.1} to stabilize as illustrated in Figure 9(b). Even though U_{meas.1} and U_{meas.2} are not significantly influenced by this sudden disturbance, they counteract each other's responses as depicted in Figure 9(c). U_{meas.1} attains its maximum overshoot of 0.58% in 0.089 seconds, whereas U_{meas.2} declines to an undershoot of 0.15% in 0.029 seconds, as measured from the instant the disturbance is applied as listed in Table 1. Both converter stations' DC voltage responded identically to the disturbance. However, U_{dc-meas.1} has a significantly larger undershoot than U_{dc-meas.2} see Figure 9(d).

Table 1. Transient response analysis of Pref.1 disturbance

Measured variable	MPOS%/US%		t_{\max}/t_{\min} (sec.)		t_{sett}/t to SS (sec.)		SSE (PU)		CF%	
	Station 1	Station 2	Station 1	Station 2	Station 1	Station 2	Station 1	Station 2	Station 1	Station 2
P	-17.5536	12.4963	1.6276	1.6101	0.0366	0.6977	-0.0011	0.09406	0.9699	-
Q	3.885494	-16.5367	1.5349	1.5882	1.5477	2.046	-0.0007	-0.0001	-	-
U	0.58288	-0.15269	1.5896	1.5296	0.4448	0.40319	0.00284	0.00052	-	-
U _{dc}	-4.17894	-3.73115	1.5116	1.5132	1.5542	1.5857	-0.0015	-0.0003	-	-

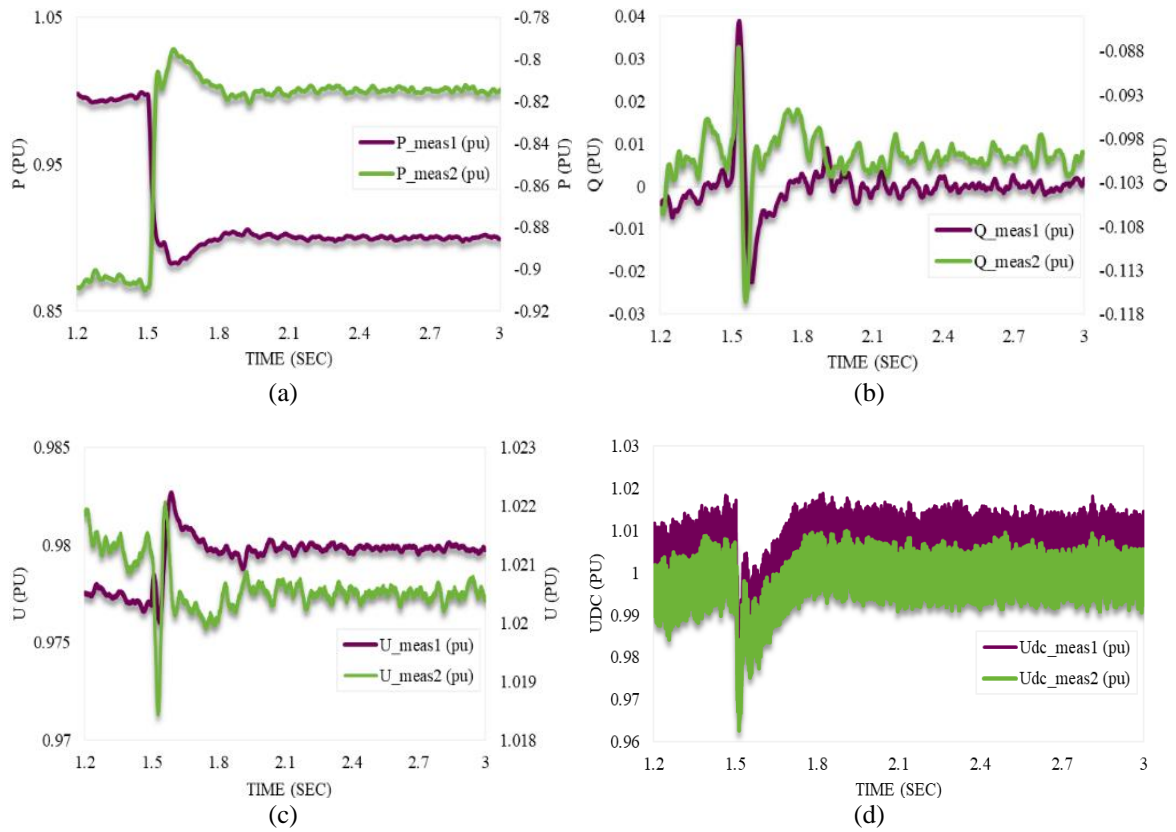


Figure 9. The measured: (a) active power, (b) reactive power, (c) RMS AC voltage, and (d) DC voltage at each converter station due to a sudden 0.1 pu disturbance in Pref.1 at 1.5 sec. in the studied model

5.3. Case 2: applied disturbance in the reference reactive power of station 1 (Qref.1)

In case 2, a disturbance on the reactive power of station 1 is applied, and the response at each converter station is analyzed. Figure 10 illustrates the response of active power, reactive power, RMS AC voltage, and DC voltage at each converter station due to this disturbance. Table 2 lists the transient response analysis of Qref.1 disturbance. As shown in Figure 10, the measured active power at both converter stations counteracts their response to that disturbance. Pmeas1 falls to an undershoot of 2%, but Pmeas2 attains its overshoot by about the same proportion see Figure 10(a). Both converter stations react identically to the disturbance in terms of reactive power as shown in Figure 10(b). However, the undershoot of Qmeas1 is greater than that of Qmeas2. The reactive power at the station in which the disturbance is applied precisely follows this variation with a CF of 0.97, but the reactive power at the other station is only minimally influenced initially before returning to its steady state see Table 2. Within 0.097 seconds, the RMS AC voltage at the station in which the disturbance in reactive power is provided increases rapidly to compensate for this decrease. In contrast, the RMS AC voltage at the other station oscillates slightly for 0.392 seconds before returning to a constant state as illustrated in Figure 10(c). DC voltage waveforms at both converter stations have almost the same response to the applied disturbance in Qmeas1 see Figure 10(d).

Table 2. Transient response analysis of Qref.1 disturbance

Measured variable	MPOS%/US%		t _{max} /t _{min} (sec.)		t _{set} /t to SS (sec.)		SSE (PU)		CF%	
	Station 1	Station 2	Station 1	Station 2	Station 1	Station 2	Station 1	Station 2	Station 1	Station 2
P	-2.54527	2.79841	1.5539	1.5604	1.5704	1.57578	0.00024	-0.0014	-	-
Q	-46.9798	-5.26913	1.5379	1.5928	1.5587	1.15948	-0.0002	0.00017	0.9676	-
U	1.600471	0.19083	1.5399	1.5977	0.1701	0.39281	0.01011	-5E-05	-	-
U _{dc}	1.549165	1.54917	1.5092	1.8712	0.1956	0.66444	0.00019	1.5E-05	-	-

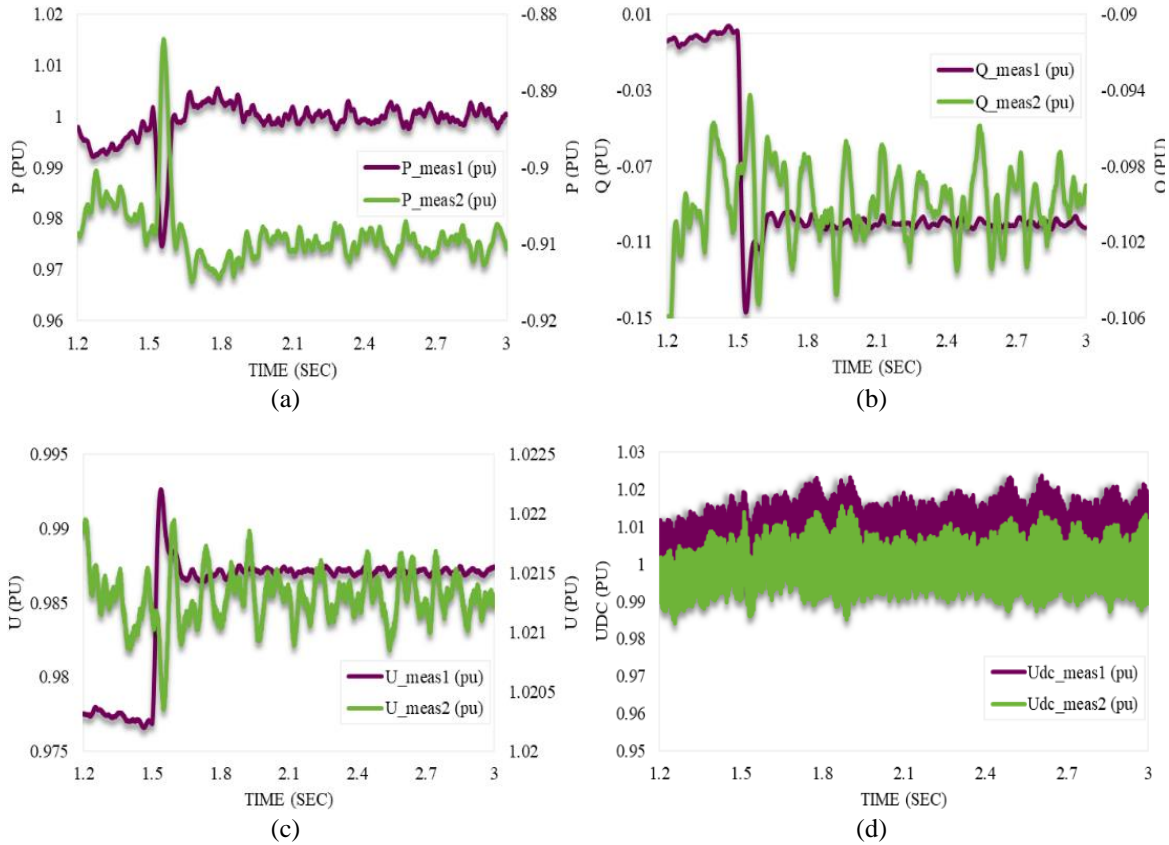


Figure 10. The measured: (a) active power, (b) reactive power, (c) RMS AC voltage, and (d) DC voltage at each converter station due to a sudden 0.1 pu disturbance in Q-ref.1 at 1.5 sec. in the model

5.4. Case 3: applied disturbance in the reference DC voltage of station 2 (Ud-ref.2)

In this case, a disturbance on the reference of the DC voltage of station 2 is applied, and the response at each converter station will be recorded and analyzed. Figure 11 illustrates the response of active power, reactive power, RMS AC voltage, and DC voltage at each converter station. Table 3 summarizes the transient response analysis of Ud-ref.2 disturbance. In contrast to Pmeas1’s 10% overshoot, Pmeas2’s 12% undershoot counteracts this effect. However, each of them needs 0.48 seconds to restore stability see Figure 11(a) and Table 3. As listed in Table 3, the reactive power at the first station, Qmeas1, grows to 6.65% overshoot while the reactive power at the second station, Qmeas2, decreases to 19.5% undershoot. Although Qmeas1 achieves steady state 0.5 seconds before Qmeas2, its steady state inaccuracy is greater than that of Qmeas2 as illustrated in Figure 11(b). In contrast to the active and reactive power response at the two converter stations, Umeas1 has recorded a greater response than Umeas2. Umeas1 decreases to a 1% undershoot, whereas Umeas1 climbs to a 0.4% overshoot see Table 3. However, Umeas2 requires more time than Umeas1 to attain its steady state see Figure 11(c). The DC voltage waveform at both converter stations responds almost identically to the disturbance supplied to Ud-ref.2, although the undershoot of Ud-ref.2 is more significant than that of converter station 1 as shown in Figure 11(d). In addition, the DC voltage at station 2 follows the variation in its reference value with a high CF of 0.9574.

Table 3. Transient response analysis of Udref.2 disturbance

Measured variable	MPOS%/US%		t _{max} /t _{min} (sec.)		t _{set} /t to SS (sec.)		SSE (PU)		CF%	
	Station 1	Station 2	Station 1	Station 2	Station 1	Station 2	Station 1	Station 2	Station 1	Station 2
P	10.84429	-12.1285	1.539	1.5507	1.999	1.9843	0.00065	-0.0095	-	-
Q	6.651196	-19.4999	1.533	1.6636	1.7597	0.71726	-0.0196	-0.0004	-	-
U	-1.04936	0.37222	1.5321	1.5107	0.7598	0.9	0.00019	0.00161	-	-
U _{dc}	-14.9539	-40.8641	1.819	1.819	0.6	1.94578	-0.1096	-0.0992	-	0.9574

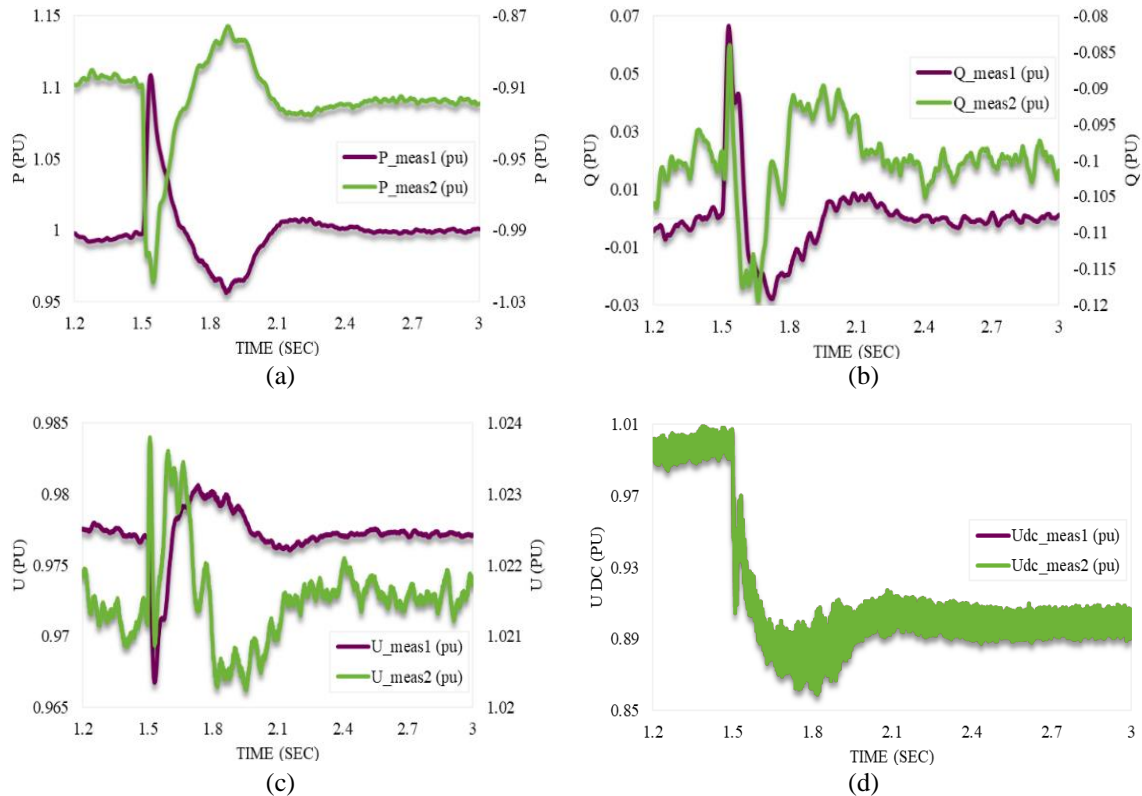


Figure 11. The measured: (a) active power, (b) reactive power, (c) RMS AC voltage, and (d) DC voltage at each converter station due to a sudden 0.1 pu disturbance in $U_{\text{d-ref.2}}$ at 1.5 sec. in the model

6. CONCLUSION

In this article, two AC networks with different frequencies are interconnected using a VSC-HVDC system including three arms-NPC converters. The system components, and vector control topology are simulated using MATLAB/Simulink simulations. Several control modes such as varying active/reactive powers and DC bus voltage are also studied. By adjusting the controller's settings, the input active power, reactive power, and DC voltage are varied in discrete steps. Active and reactive power disturbances are applied to the first converter station, while DC voltage disturbance is applied to the second converter station. The characteristics of active/reactive power and AC/DC voltage at both converter stations are studied by analyzing their transient responses. The results show that the AC voltage and active/reactive power of both converter stations counteract each other's responses. On the other hand, the DC voltage at both converter stations always responds identically to different disturbances. In addition, the system control performs well in terms of stability and robustness during these disturbances. It resumes its steady state quickly within 0.7 sec.




REFERENCES

- [1] J. Zhu *et al.*, "Inertia emulation and fast frequency-droop control strategy of a point-to-point VSC-HVdc transmission system for asynchronous grid interconnection," *IEEE Transactions on Power Electronics*, vol. 37, no. 6, pp. 6530–6543, Jun. 2022, doi: 10.1109/TPEL.2021.3139960.
- [2] Y. Hu, X. Wang, T. Huang, X. Lei, and T. Wang, "An optimal frequency control method of asynchronous power grid considering multi-HVDC emergency power support," *IEEE Access*, vol. 10, pp. 78011–78021, 2022, doi: 10.1109/ACCESS.2022.3192569.
- [3] L. Shi, G. P. Adam, R. Li, and L. Xu, "Enhanced control of offshore wind farms connected to MTDC network using partially selective DC fault protection," *IEEE Journal of Emerging and Selected Topics in Power Electronics*, vol. 9, no. 3, pp. 2926–2935, 2021, doi: 10.1109/JESTPE.2020.2985129.
- [4] F. Muzi, "Supergrids and the new challenges to face," *Proceedings of the 6th IASTED Asian Conference on Power and Energy Systems, AsiaPES 2013*, no. April 2013, pp. 142–146, 2013, doi: 10.2316/P.2013.800-098.
- [5] M. Wang *et al.*, "Review and outlook of HVDC grids as backbone of transmission system," *CSEE Journal of Power and Energy Systems*, vol. 7, no. 4, pp. 797–810, 2021, doi: 10.17775/CSEEJPES.2020.04890.
- [6] W. Du, Q. Fu, and H. Wang, "Comparing AC dynamic transients propagated through VSC HVDC connection with master-slave control versus DC voltage droop control," *IEEE Transactions on Sustainable Energy*, vol. 9, no. 3, pp. 1285–1297, 2018, doi: 10.1109/TSTE.2017.2781237.




- [7] P. Simiyu, A. Xin, G. T. Bitew, M. Shahzad, W. Kuniyu, and L. K. Tuan, "Review of the DC voltage coordinated control strategies for multi-terminal VSC-MVDC distribution network," *The Journal of Engineering*, vol. 2019, no. 16, pp. 1462–1468, Mar. 2019, doi: 10.1049/joe.2018.8841.
- [8] R. Imanwan, F. F. da Silva, C. L. Bak, and T. C. Bregnhøj, "An initial topology of multi-terminal HVDC transmission system in Europe: A case study of the North-Sea region," in *2016 IEEE International Energy Conference (ENERGYCON)*, Apr. 2016, pp. 1–6, doi: 10.1109/ENERGYCON.2016.7513880.
- [9] A. Raza, X. Dianguo, S. Xunwen, L. Weixing, and B. W. Williams, "A novel multiterminal VSC-HVdc transmission topology for offshore wind farms," *IEEE Transactions on Industry Applications*, vol. 53, no. 2, pp. 1316–1325, 2017, doi: 10.1109/TIA.2016.2628901.
- [10] M. A. Hannan *et al.*, "Advanced control strategies of VSC based HVDC transmission system: issues and potential recommendations," *IEEE Access*, vol. 6, pp. 78352–78369, 2018, doi: 10.1109/ACCESS.2018.2885010.
- [11] B. R. Andersen, L. Xu, and K. T. G. Wong, "Topologies for VSC transmission," in *IEE Conference Publication*, 2002, vol. 2001, no. 485, pp. 298–304, doi: 10.1049/cp:20010559.
- [12] G. Kalcon, G. P. Adam, O. Anaya-Lara, G. Burt, and K. L. Lo, "Analytical efficiency evaluation of two and three level VSC-HVDC transmission links," *International Journal of Electrical Power and Energy Systems*, vol. 44, no. 1, pp. 1–6, 2013, doi: 10.1016/j.ijepes.2012.07.018.
- [13] H. Liu, Z. Xu, and Z. Gao, "A control strategy for three-level VSC-HVDC system," in *IEEE Power Engineering Society Summer Meeting*, 2002, vol. 1, no. SUMMER, pp. 480–485, doi: 10.1109/PESS.2002.1043280.
- [14] H. Mahmoudi, M. Aleenejad, and R. Ahmadi, "Modulated model predictive control of modular multilevel converters in VSC-HVDC systems," *IEEE Transactions on Power Delivery*, vol. 33, no. 5, pp. 2115–2124, 2018, doi: 10.1109/TPWRD.2017.2727478.
- [15] H. You and X. Cai, "A three-level modular DC/DC converter applied in high voltage DC grid," *IEEE Access*, vol. 6, pp. 25448–25462, 2018, doi: 10.1109/ACCESS.2018.2829703.
- [16] K. Shinoda, A. Benchaib, J. Dai, and X. Guillaud, "DC voltage control of MMC-based HVDC grid with virtual capacitor control," in *2017 19th European Conference on Power Electronics and Applications, EPE 2017 ECCE Europe*, 2017, vol. 2017-January, p. P.1-P.10, doi: 10.23919/EPE17ECCEEurope.2017.8099097.
- [17] A. Pragati, M. Mishra, P. K. Rout, D. A. Gadanayak, S. Hasan, and B. R. Prusty, "A comprehensive survey of HVDC protection system: fault analysis, methodology, issues, challenges, and future perspective," *Energies*, vol. 16, no. 11, p. 4413, May 2023, doi: 10.3390/en16114413.
- [18] R. H. Chandio *et al.*, "Control and protection of MMC-based HVDC systems: A review," *Energy Reports*, vol. 9, pp. 1571–1588, 2023, doi: 10.1016/j.egyr.2022.12.056.
- [19] J. Lyu, X. Cai, and M. Molinas, "Optimal design of controller parameters for improving the stability of MMC-HVDC for wind farm integration," *IEEE Journal of Emerging and Selected Topics in Power Electronics*, vol. 6, no. 1, pp. 40–53, Mar. 2018, doi: 10.1109/JESTPE.2017.2759096.
- [20] M. Khatir, S. A. Zidi, S. Hadjeri, and M. K. Fellah, "Dynamic performance of a back-to-back HVDC station based on voltage source converters," *Journal of Electrical Engineering*, vol. 61, no. 1, pp. 29–36, Jan. 2010, doi: 10.2478/v10187-010-0004-9.
- [21] A. K. Biswas, S. I. Ahmed, S. K. Akula, and H. Salehfar, "High voltage AC (HVAC) and high voltage DC (HVDC) transmission topologies of offshore wind power and reliability analysis," *IEEE Green Technologies Conference*, vol. 2021-April, no. March, pp. 271–278, 2021, doi: 10.1109/GreenTech48523.2021.00051.
- [22] R. Ryndzionek and Ł. Sienkiewicz, "Evolution of the HVDC link connecting offshore wind farms to onshore power systems," *Energies*, vol. 13, no. 8, 2020, doi: 10.3390/en13081914.
- [23] A. Yahiaoui, K. Iffouzar, K. Ghedamsi, and K. Himour, "Dynamic performance analysis of VSC-HVDC based modular multilevel converter under fault," *Journal Europeen des Systemes Automatises*, vol. 54, no. 1, pp. 187–194, Feb. 2021, doi: 10.18280/jesa.540121.
- [24] T. Navpreet *et al.*, "Voltage source converters as the building block of HVDC and FACTS technology in power transmission system: a simulation based approach," *Pelagia Research Library Advances in Applied Science Research*, vol. 3, no. 5, pp. 3263–3278, 2012, [Online]. Available: www.pelagiaresearchlibrary.com.
- [25] A. Khillio and S. S. Patnaik, "Performance analysis of 6-pulse HVDC-VSC using particle swarm optimization (PSO) based controller in d-q reference frame under transient AC fault conditions," in *2020 5th IEEE International Conference on Recent Advances and Innovations in Engineering, ICRAIE 2020 - Proceeding*, Dec. 2020, no. 1, pp. 1–6, doi: 10.1109/ICRAIE51050.2020.9358345.
- [26] R. Shah, J. C. Sánchez, R. Preece, and M. Barnes, "Stability and control of mixed AC-DC systems with VSC-HVDC: a review," *IET Generation, Transmission and Distribution*, vol. 12, no. 10, pp. 2207–2219, May 2018, doi: 10.1049/iet-gtd.2017.1140.

BIOGRAPHIES OF AUTHORS






Reem Ahmed Mostafa    was born in Cairo, Egypt in 1998. She received B.Sc. in energy and renewable energy engineering from the faculty of engineering at Ain Shams University (ASU) in 2021. She is currently a teaching assistant with the department of Electrical Power and Machines-at the higher institute of engineering-El'Shorouk City, Egypt. She can be contacted at email: reem.ahmed.mos@gmail.com.






Adel Emary Salem    is currently the head of the control sector at the National Energy Control Center, Egyptian Electricity Transmission Company (EETC). He received B.Sc. M.Sc. and Ph.D. degrees in electrical power engineering Ain Shams University (ASU) in 1991, 2000, and 2007 respectively. He can be contacted at email: adelaly188@yahoo.com.



Ahmed Sayed Abdelhamid    was born in Cairo, Egypt in 1986. He received B.Sc. M.Sc. and Ph.D. degrees in electric power engineering from the higher institute of engineering El'Shorouk Academy in 2008, Arab Academy for Science Technology and Maritime Transport (AASTMT) in 2015, and Cairo University in 2019, respectively. He is currently a lecturer of electrical power systems with the department of Electrical Power and Machines-at the higher institute of engineering - El'Shorouk Academy. His fields of interest include electric power system: analysis, stability, economics, optimization, distribution, renewable energy integration, transformers, power electronics, and reliability. He can be contacted at email: eng_ahmed_sayed2010@yahoo.com.



Prof. Dr. Mohamed EL-Shimy Mahmoud Bekhet    is currently a professor of electrical power systems with the department of Electrical Power and Machines-Faculty of Engineering - Ain Shams University. He is also an electromechanical specialist, a freelance trainer, technical advisor, and a member of many associations and professional networks. He is a technical reviewer with some major journals and conferences. His fields of interest include electric power system: analysis, stability, economics, optimization, distribution, renewable energy integration, and reliability. He can be contacted at email: mohamed_bekhet@eng.asu.edu.eg.